Ceramics International 46 (2020) 4992–4997

Contents lists available at ScienceDirect

Ceramics International

journal homepage: www.elsevier.com/locate/ceramint

Pure and cerium-doped zinc orthosilicate as a pigment for thermoregulating coatings

V.V. Baghramyan[a], A.A. Sargsyan[a], N.B. Knyzyan[a], V.V. Harutyunyan[b], A.H. Badalyan[b], N.E. Grigoryan[b], A. Aprahamian[b,c], K.V. Manukyan[c,*]

[a] M.G. Manvelyan Institute of General and Inorganic Chemistry, National Academy of Sciences, 10 Argutyan Str., 0051, Yerevan, Armenia
[b] Alikhanian National Science Laboratory, 2, Alikhanian Brothers Str., Yerevan, 0036, Armenia
[c] Nuclear Science Laboratory, Department of Physics, University of Notre Dame, Notre Dame, IN, 46556, USA

ARTICLE INFO

Keywords:
Zinc orthosilicate
Hydrothermal-microwave synthesis
Doping
Diffuse-reflection
Radiation resistance
Thermoregulating coatings

ABSTRACT

Microwave-assisted hydrothermal synthesis followed by high-temperature (1050 °C) calcination was used to prepare pure and cerium-doped zinc orthosilicate (Zn_2SiO_4) pigments. Nanoscale Zn_2SiO_4 and Ce–Zn_2SiO_4 powders were blended with potassium silicate (K_2SiO_3) and then applied to the aluminum substrate to obtain thermoregulating coatings. Electron beams with different energies were used to irradiate nanoscale pigment powders and coatings. X-ray diffraction (XRD), scanning electron microscopy (SEM), and transition electron microscopy (TEM) were used to characterize the phase composition, morphology, and atomic-level structure of materials. The diffuse reflectance and absorption measurements of materials before and after irradiation indicated that Ce–Zn_2SiO_4-based coatings exhibit better radiation resistance compared to pure Zn_2SiO_4. Simple and straightforward preparation, as well as high radiation resistance, make Ce–Zn_2SiO_4-based thermoregulating coatings excellent candidates for space vehicles.

1. Introduction

Ceramic pigments (ZnO, TiO_2, Y_2O_3, stabilized-ZrO_2) with high reflectivity in the solar spectrum and high emissivity in the infrared range mixed with binder phases (epoxies, acrylics, silicones, polyurethanes) are applied on the external surfaces of spacecraft or satellites to maintain the thermal balance and provide stable power consumption for the instruments on board [1]. These coatings are subjected to high fluxes of radiation (electrons, protons, ultraviolet, X-rays) and mechanical damage from space debris as well as extreme thermal cycling [2–7]. High energy electron and proton fluxes combined with short-wavelength (< 230 nm) solar radiation generate atomic oxygen by dissociation of the double bond in oxygen molecules at low Earth orbits [1,8]. Such harsh conditions significantly influence the thermal and optical properties of coatings and may result in substantial mechanical damage [1].

The ideal coatings should have high melting points, low thermal conductivity, excellent chemical stability, no phase transitions at the operating temperatures, a coefficient of thermal expansion similar to the substrate, and high adhesion to the substrate. The absorption coefficient of solar radiation (α_s) and the light reflectance of the coatings are essential characteristics of absorption and heat emission for spacecraft surfaces. Coatings with α_s ~10–30% and reflectance of ~0.8–0.9 can efficiently remove the excess heat from the surface of a spacecraft. Thermoregulating coatings with white pigments ZnO, TiO_2, Y_2O_3, and stabilized-ZrO_2 satisfy these requirements [5,9]. However, the pigments in the coatings are affected by proton or electron radiation, while the organic binders undergo degradation with ultraviolet irradiation [1–7].

This work reports on a new method to develop zinc orthosilicate (Zn_2SiO_4) – potassium silicate (K_2SiO_3) composites with high electron radiation tolerance and reflectivity for solar light. Zn_2SiO_4 exists in α- and β-crystalline phases [10]. β-Zn_2SiO_4 is metastable and transforms into the α-phase at high temperatures. α-Zn_2SiO_4 exhibits no solid-state phase transitions below its melting point of 1550 °C and is a suitable phosphor host-matrix that possesses excellent luminescent properties in the blue, green, and red spectral regions [11–17]. Mn-doped zinc silicate (Zn_2SiO_4: Mn^{2+}) has been used extensively in industry for manufacturing lighting devices since the 1930s [10]. This ceramic material is also being considered for use in lithium-ion batteries [18–20], as well as for making pigments [21–24] and adsorbents [25–27].

Zn_2SiO_4-based ceramics is conventionally produced by solid-state reactions of well-mixed ZnO and SiO_2 powders at temperatures of 1100–1500 °C for periods ranging from 2 to 4 h [24,28,29]. Solid-state

* Corresponding author.
E-mail address: kmanukya@nd.edu (K.V. Manukyan).

https://doi.org/10.1016/j.ceramint.2019.10.239
Received 13 May 2019; Received in revised form 25 October 2019; Accepted 25 October 2019
Available online 28 October 2019

synthesis results in large irregular particles with a broad size distribution (1–10 μm). Solvothermal synthesis methods result in the formation of α-Zn_2SiO_4 nanorods at temperatures below 370 °C. The crystallinity of these products, however, is considerably lower than those prepared by solid-state reactions [19,20,26,30,31]. Supercritical water conditions (temperatures above 370 °C and pressures higher than 22.1 MPa) enable the synthesis of α-Zn_2SiO_4 at shorter reaction times than solvothermal methods [32,33]. The sol-gel formulations allow for the preparation of fine particles with controlled shape and narrow size distributions under atmospheric pressure and room temperature conditions [16,22,34–37]. The products, however, should be calcinated at temperatures higher than 800 °C to provide the formation of highly crystalline materials.

Investigations of different pigments with high radiation resistance and new formulations that allow the elimination of organic binders is the goal of this study with the expectation of significant improvements in the service life of thermoregulating coatings on spacecraft. This work reports a simple preparation of Zn_2SiO_4-based thermoregulating coatings with a silicate (K_2SiO_3) binder. A microwave-assisted hydrothermal synthesis was used to prepare pure and ceria-doped Zn_2SiO_4 nanoscale pigments for coatings. Both the pigments and the coatings were irradiated using high energy electron beams and characterized to evaluate the effect of radiation on the structure and properties of materials.

2. Experimental

2.1. Synthesis and processing

Na_2SiO_3 and K_3SiO_3 reactants (with 99% purity) are used for the synthesis of Zn_2SiO_4-based pigments and binders for thermoregulating coatings. Aqueous solutions of zinc chloride ($ZnCl_2$, 99.5%) and Na_2SiO_3 with 1.0 mol/l concentrations were mixed and irradiated in a MS-6 “VOLTA” microwave oven (2.45 GHz frequency) for 1.5–3.5 h. The maximum temperature during the synthesis was measured to be ~240 °C. Cerium (III) nitrate hexahydrate (99.0%) was added to the solutions for the preparations of 3% by weight Ce–Zn_2SiO_4 pigments. This concentration was selected to ensure doping the material and not to form a second phase. After microwave irradiation, the precipitates were filtered and washed with warm deionized water to remove NaCl by-products and then dried at 110 °C. The pigment powders were calcined at 1050 °C in a muffle furnace for 1 h. The developed synthesis procedure is reproducible. Each type of material was prepared at least in three different batches. The phase composition and morphology of batches were shown to be identical. To prepare thermal barrier coatings, a mixture of pigment and binder (solution of K_2SiO_3 with silica modulus of 3.3–3.8 and density 1.17–1.18 g/cm^3) with 1:1 wt ratio was stirred in a planetary mixer with agate balls for 1 h to obtain a homogeneous slurry. The slurry was applied to aluminum (grade 3003) disks then allowed to solidify at room temperature to obtain ~150 μm thick coatings.

2.2. Irradiation

Pallets (~3 mm thick discs with a diameter of 20 mm) made from compressed pigment powders were irradiated with high-energy electron beams. The irradiation of pigment pellets and thermoregulating coatings was performed at the Alikhanyan National Science Laboratory using the 75 MeV LUex linear electron accelerator. Electron beams of 5 and 20 MeV energies and fluence of 10^{17} electrons/cm^{-2} were used. This corresponds to an exposure of more than 15 years in the Earth's radiation belt. The average flux density of electrons was kept at approximately 10^{12} cm^{-2}s^{-1} to avoid heating the samples during irradiation.

2.3. Characterization

The crystallinity and phase compositions of the materials were investigated by X-ray diffraction (XRD) analysis with Ni-filtered CuKα radiation (D8 Advance, Bruker), operated at 40 kV and 40 mA with a step size of 0.025° and a counting time of 5 s for the angular range of 20–70° (2θ). Nitrogen adsorption isotherms of the synthesized and calcined pigment powders were measured using an AccuSorb 2100E instrument (Micromeritics) at −196 °C. The samples were degassed at 250 °C for 12 h under reduced pressure before measurements. The specific surface area of samples was calculated from the adsorption curve according to the Brunauer-Emmett-Teller (BET) method. Scanning (SEM) and transmission electron microscopes (TEM) were used to characterize the composition and morphology of the products as well as their atomic structure. Microstructural analysis was conducted in a field emission SEM Magellan 400 (FEI) microscope. A Titan (FEI) TEM with a resolution of 0.136 nm in scanning TEM mode and an information limit of about 0.1 nm at high-resolution TEM mode was also used. Diffuse reflectance/absorption of the coatings was measured within the range of 200–950 nm. Optical absorption/diffuse reflectance measurements of pigment powders and coatings were performed using a UV–Visible - Near-IR (Jasco) spectrometer.

3. Results and discussions

3.1. Synthesis of pigments

Fig. 1 shows the XRD patterns for Zn_2SiO_4 pigment powders prepared with 1.5 and 3.5 h of microwave irradiation. The material prepared with 1.5 h of irradiation exhibits broad diffraction peaks of α-Zn_2SiO_4 (PDF card # 37-1485) rhombohedral structure with a space group of R–3, and cell constant a = b = 1.395 nm, c = 0.9312 nm (Fig. 1a). The XRD pattern also contains peaks for SiO_2 (PDF card #14-0653) and ZnO (PDF card #65-3411) phases along with some unidentified weak lines. The positions of the ZnO peaks are shifted by ~0.8° to a lower angular range indicating non-equilibrium defective structures. The intensities of diffraction peaks for the α-Zn_2SiO_4 sample after 3.5 h of microwave-irradiation are significantly higher (Fig. 1b). The positions of ZnO peaks are shifted by 0.6°, but the intensity ratio of those lines has changed in comparison to the previous sample. XRD patterns of materials prepared after 3.5 h of microwave irradiation also exhibit less intense peaks for SiO_2 and the unidentified phase. Adding

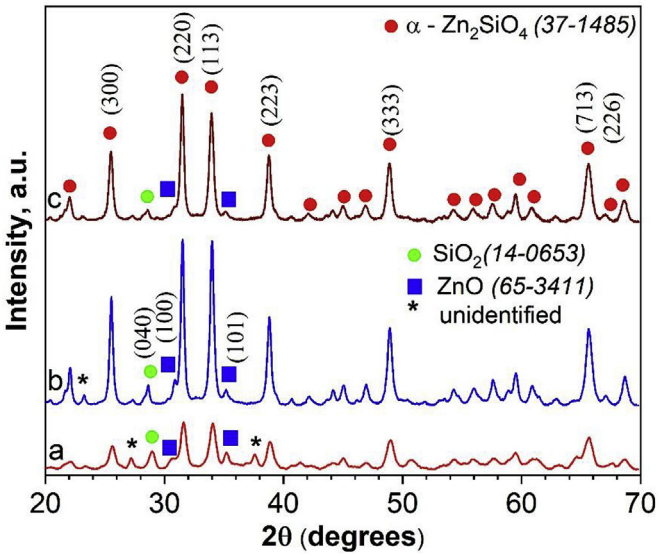

Fig. 1. XRD patterns of Zn_2SiO_4 (a, b) and Ce–Zn_2SiO_4 (c) synthesized under microwave irradiation at durations of 1.5 (a) and 3.5 h (b, c).

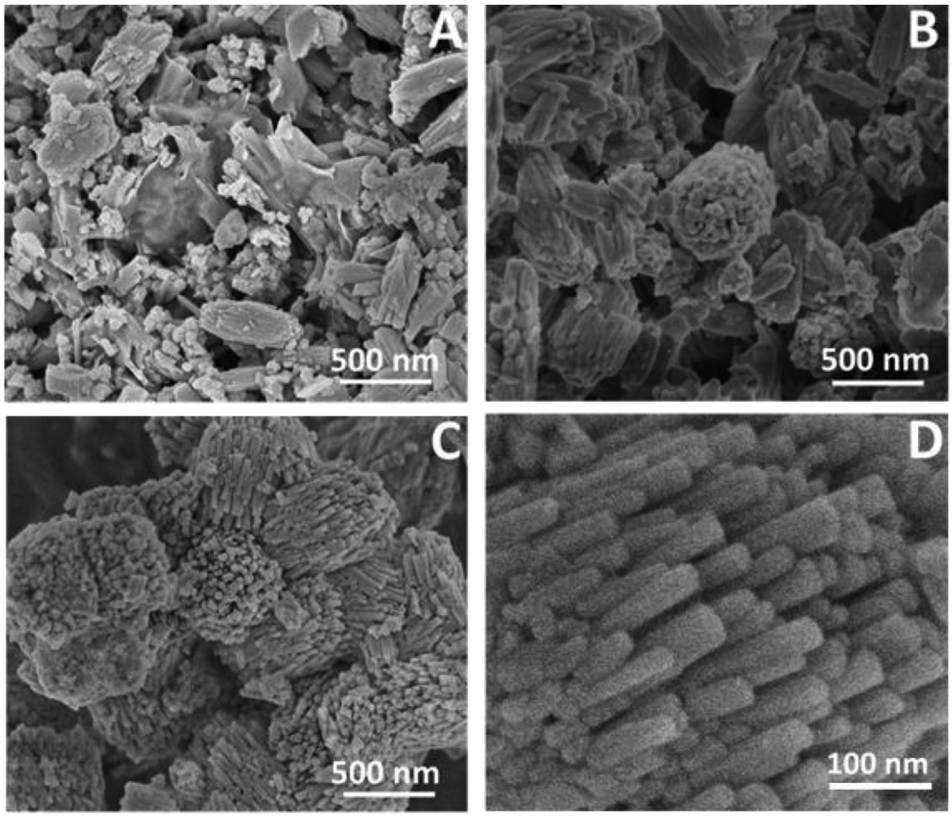

Fig. 2. SEM images of Zn_2SiO_4 (A, B) and Ce–Zn_2SiO_4 (C, D) synthesized under microwave irradiation for durations of 1.5 h (A) and 3.5 h (B–D).

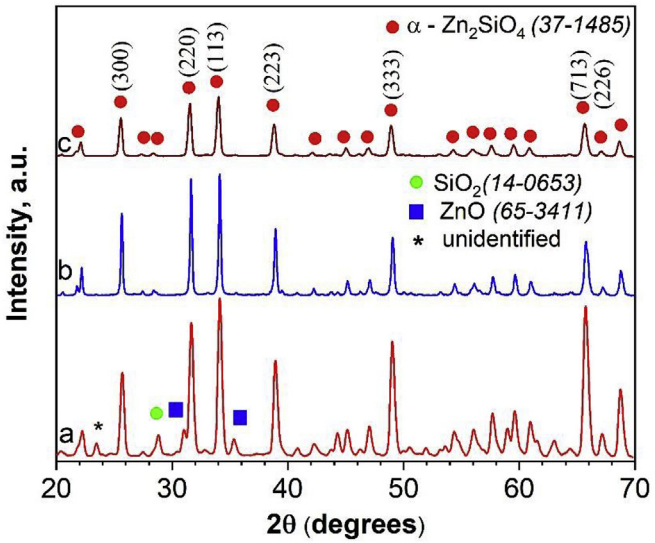

Fig. 3. XRD patterns of Zn_2SiO_4 (a) and Ce–Zn_2SiO_4 (b) samples calcined at 1050 °C as well as Ce–Zn_2SiO_4 subjected to 20 MeV electron irradiation with 10^{17} electron/cm^{-2} fluence (c).

Ce to the synthesis process (3.5 h of microwave irradiation) reduces the amount of unreacted ZnO and SiO_2 and increases their conversion to Zn_2SiO_4. The introduction of Ce also helps to eliminate the unidentified phase.

BET measurements indicate the surface area for Zn_2SiO_4 pigments were 18 and 14 m^2/g for 1.5 and 3.5 h of microwave irradiation, respectively. The Ce–Zn_2SiO_4 product prepared with 3.5 h of irradiation also exhibits similar BET surface area (13 m^2/g). Fig. 2 shows the morphology of Zn_2SiO_4 and Ce–Zn_2SiO_4 samples prepared by microwave irradiation with a duration of 1.5 and 3.5 h. Fig. 2A shows that after 1.5 h of microwave irradiation, the product contains three different morphological features: rice-like aggregates with sizes of 300–500 nm, agglomerates of fine (~100 nm) particles and large (500–1000 nm) irregular crystals with a smooth surface. Close inspection suggests that the rice-like particles are bundles of nanorods consisting of Zn, Si, and O, as revealed by local elemental analysis (not shown). The nanoparticle agglomerates primarily contain Zn and O; while the larger irregular crystals contain Si and O. The results of local microanalysis suggest that the rice-like particles are Zn_2SiO_4, whereas nanoparticles and larger crystals are ZnO and SiO_2, respectively. More prolonged microwave irradiation (3.5 h) results in significant growth of the rice-like aggregates (Fig. 2B), while nanoscale particles and the larger irregular crystals almost disappear from the product. Fig. 2C indicates that cerium doping helps to obtain products with more uniform morphology. A closer look at the aggregates reveals that the nanorods have a ~50 nm diameter and 100–150 nm length (Fig. 2D). This image also suggests that nanorods nucleated at the same origin then vertically grew during microwave-assisted synthesis. SEM imaging suggests that adding Ce helps the growth of Zn_2SiO_4 nanorods along a preferential orientation.

3.2. Processing and irradiation

High-temperature calcination was used to achieve the complete conversion of reactants and improve the crystallinity of products. The XRD pattern from the calcined Zn_2SiO_4 sample prepared by 3.5 h of microwave irradiation indicates that calcination has little effect on the reaction of ZnO with the SiO_2 byproduct (Fig. 3a). The calcined product contains both those impurities along with a small amount of an unidentified phase. The calcination of the Ce–Zn_2SiO_4 sample contributes towards the full conversion of intermediate products to α-Zn_2SiO_4 (Fig. 3b). All the diffraction lines are indexed to the pure phase of $\alpha - Zn_2SiO_4$ with rhombohedral structure, and no peaks from other phases can be detected. An XRD pattern of calcined then electron beam

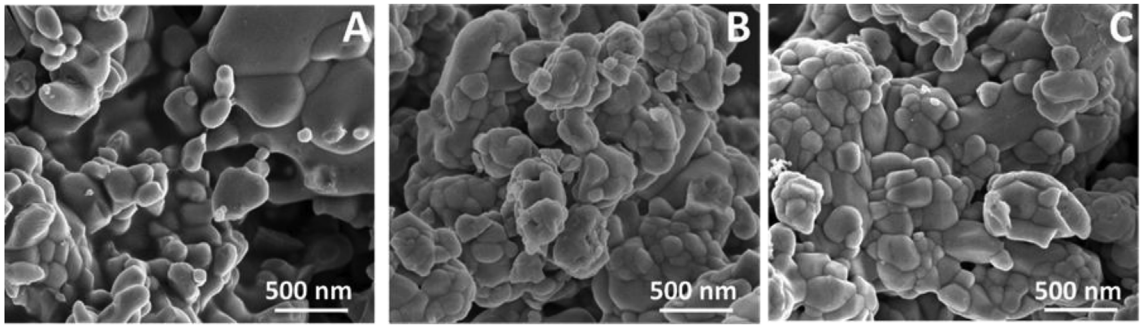

Fig. 4. SEM images of Zn_2SiO_4 (A) and Ce–Zn_2SiO_4 (B) samples calcined at 1050 °C as well as Ce–Zn_2SiO_4 subjected to 20 MeV electron irradiation with 10^{17} electrons/cm^{-2} fluence (C).

irradiated material (20 MeV and 10^{17} electron/cm^{-2} fluence) indicates that it maintains the $\alpha - Zn_2SiO_4$ structure, but some broadening of diffraction peaks occurs (Fig. 3c).

BET measurements show that calcined and irradiated powders have ~1 m^2/g surface area. SEM imaging (Fig. 4A) shows that the calcined Zn_2SiO_4 (prepared by 3.5 h microwave irradiation) sample consists of sintered particles with a broad size distribution (100–2000 nm). Calcined Ce–Zn_2SiO_4 samples (prepared by 3.5 h microwave irradiation) composed of sintered near-spherical particles form agglomerates with sizes of 500–1000 nm (Fig. 4B). The sizes of individual particles vary in the 200–300 nm range. We can suggest that the sintering of nanorods aggregates (Fig. 2C) results in the formation of sintered particle agglomerates. Fig. 4C shows that the electron-irradiated (20 MeV 10^{17} electron/cm^{-2} fluence) Ce–Zn_2SiO_4 sample exhibits a similar microstructure compared to the sample before irradiation (Fig. 4B).

To investigate the radiation resistance of Ce–Zn_2SiO_4, samples were subjected to TEM analysis. Fig. 5A and B shows bright-field TEM images of selected particles before and after irradiation (20 MeV electron irradiation with 10^{17} cm^{-2} fluence), respectively. These images display particles with sizes as large as 300 nm for both samples. The particles after irradiation show some grains with sizes less than 100 nm. High-resolution EDS analysis in various parts of these particles indicates similar silicon/zinc ratios suggesting that irradiation does not induce any segregation processes. Selected area diffraction patterns (Fig. 5B and C) for both particles reveal sharp diffraction rings. The indexed electron diffraction pattern suggests that both materials exhibit the structure of zinc orthosilicate. High-resolution TEM images for samples before and after irradiation are also presented in Fig. 5. Both TEM images display that the samples have a highly crystalline structure. Both images also show the high-resolution structure of nanoparticles with a d-spacing of ~0.7 nm which corresponds to the (110) crystallographic orientation of the Zr_2SiO_4 phase. The results of TEM analysis indicate that high-energy electron irradiation is not damaging the crystalline structure of Ce-doped Zn_2SiO_4 material.

3.3. Optical properties

To further evaluate the radiation resistance of the materials, the optical properties of Zn_2SiO_4 and Ce–Zn_2SiO_4 powders and coatings before and after electron irradiation were investigated using diffuse reflection/absorption spectroscopy. Since silicates have a complex structure, it is difficult to determine the defects responsible for the formation of various irradiation-induced color centers. Point defects generated upon exposure to irradiation serve as traps for electrons and

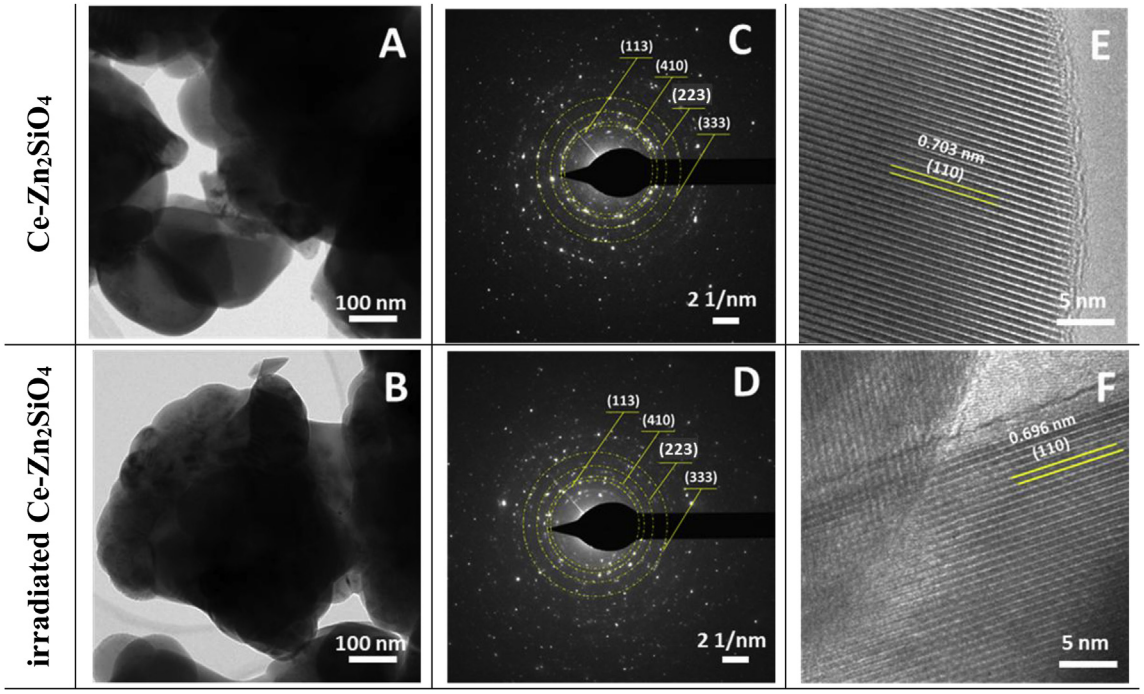

Fig. 5. Bright-field TEM images (A,B), selected area electron diffraction patterns (C,D) and high-resolution TEM images (E,F) of Ce–Zn_2SiO_4 before and after irradiation with 20 MeV electron beam and 10^{17} electrons/cm^{-2} fluence.

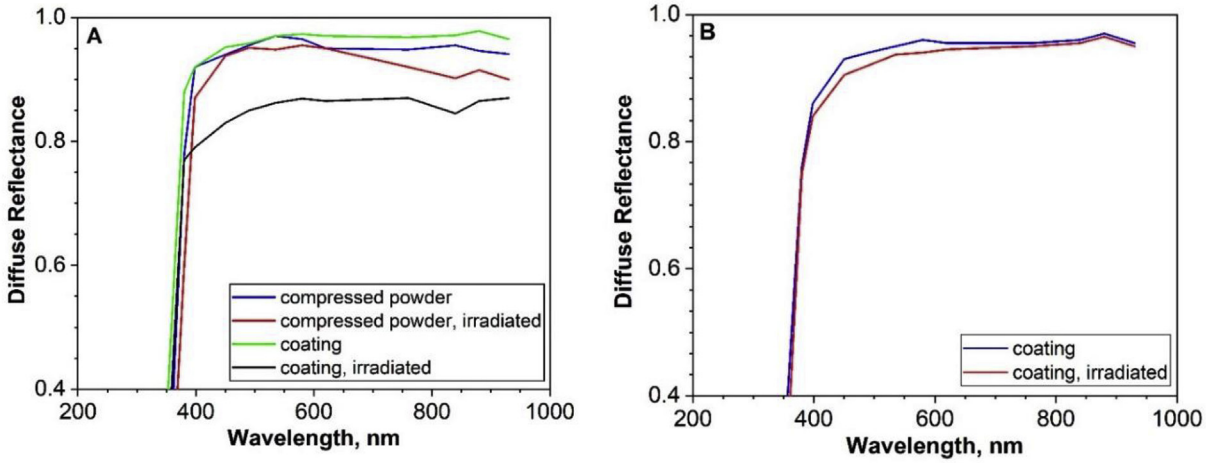

Fig. 6. Diffuse reflectance spectra of Zn_2SiO_4 (A) and Ce–Zn_2SiO_4 (B) pigments and coatings before and after electron irradiation (5 MeV and 10^{17} electrons/cm^2).

holes and become color centers. Electrons and holes fill these centers leading to an increase in the optical density of silicates. Optical density depends on the irradiation dose rate as well as on the isothermal annealing rate of the color centers.

Fig. 6A presents diffuse reflectance spectra for Zn_2SiO_4 compressed powders and coatings in the 350–950 nm region. The reflection spectra exhibit high reflectance values (above 0.93) of the powder before and after electron irradiation. The reflectance spectrum of the Zn_2SiO_4 coating on an Al substrate also exhibits similar characteristics to the powder sample. After electron irradiation (5 MeV), the reflectance of the Zn_2SiO_4 coating decreases to 0.75–0.85 in the 500–950 nm wavelength range, suggesting that high-energy electron irradiation causes significant damage to the Zn_2SiO_4 coatings.

Fig. 6B shows the diffuse reflectance spectra for Ce–Zn_2SiO_4 coatings before and after electron irradiation with the same irradiation conditions. This figure shows that irradiation weakly influences the optical characteristics of Ce–Zn_2SiO_4 coatings. The diffuse reflectance spectra for the coating before and after irradiation is practically the same. A slight decrease in reflectance can be seen only within the 400–600 nm range.

The UV–Vis–NIR absorption spectra for Ce–Zn_2SiO_4 pigments before and after irradiation show intense absorption bands in the 200–360 nm range (Fig. 7). The spectra of the irradiated pigments also exhibit some

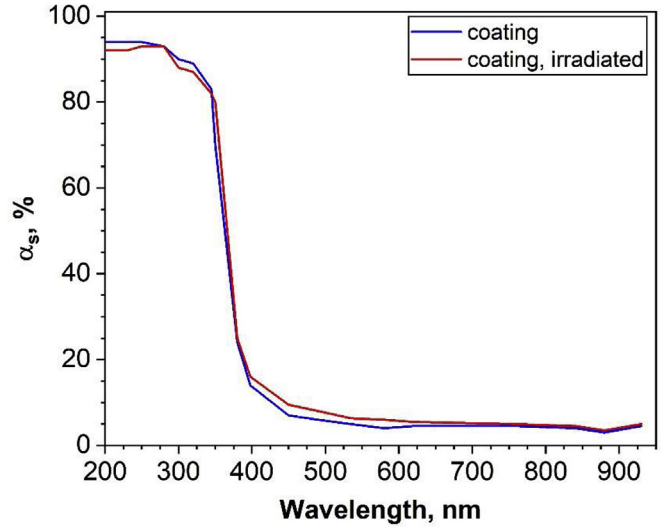

Fig. 7. UV–Vis–NIR absorption spectra of Ce–Zn_2SiO_4 pigments before and after irradiation (5 MeV and 10^{17} electrons/cm^2).

increased absorption in the 400–600 nm range. We can suggest that such small increases in absorption are attributed to the generation of small amounts of intrinsic point defects such as zinc and oxygen vacancies and their complexes (Frenkel pairs of $Zn_i^{\cdot\cdot}$ - V_{Zn}'', and O_i'' - $Vo^{\cdot\cdot}$, electron and hole centers) upon irradiation. These results show that Ce-doping significantly increases the radiation resistance of the Zn_2SiO_4-based pigments. The Ce-doping helps to produce a highly crystalline nanoscale zinc orthosilicate structure. It also stabilizes the crystal structure, most likely due to the difference between the electric field of Ce^{3+}/Ce^{4+} and Zn^{2+} cations. Such a difference could result in the reduction of the total energy of the lattice, thus making it more stable under the high-energy electron irradiation.

4. Conclusions

- Microwave-assisted hydrothermal synthesis methods allow the production of pure and Ce-doped Zn_2SiO_4. Ce-doping reduces the amount of unreacted ZnO and SiO_2 and increases their conversion to Zn_2SiO_4, as well as helps to obtain products with more uniform morphology.
- The short calcination step applied to the synthesized nanostructured products allows the preparation of highly crystalline Zn_2SiO_4 and Ce–Zn_2SiO_4 pigment powders, which can be blended with potassium silicate and then applied to aluminum substrates to function as thermoregulating coatings.
- UV-VIS-NIR absorption/reflection measurements of the electron-irradiated materials indicate that Ce–Zn_2SiO_4 exhibits better radiation resistance compared to pure Zn_2SiO_4.

Declaration of competing interest

The authors declare that they have no known competing financial interests or personal relationships that could have appeared to influence the work reported in this paper.

Acknowledgments

The work was performed with financial support in part from the International Science and Technology Center (ISTC) in the framework A-2133 grant. A. Aprahamian and K. Manukyan acknowledge financial support from the U.S. Department of Energy's (DOE) National Nuclear Security Administration (NNSA, Grant # DE-NA0003888) and the US National Science Foundation (NSF, PHY-1713857) grants. A. Aprahamian also acknowledges support from the Fulbright U.S. Scholar grant.

References

[1] M. Hołyńska, A. Tighe, C. Semprimoschnig, Coatings and thin films for spacecraft thermo-optical and related functional applications, Adv. Mater. Interfaces 5 (2018) 1–20, https://doi.org/10.1002/admi.201701644.

[2] J.A. Dever, M.V. Nathal, J.A. DiCarlo, Research on high-temperature aerospace materials at NASA Glenn research center, J. Aerosp. Eng. 26 (2013) 500–514, https://doi.org/10.1061/(ASCE)AS.1943-5525.0000321.

[3] A. Hendaoui, N. Émond, S. Dorval, M. Chaker, E. Haddad, VO_2-based smart coatings with improved emittance-switching properties for an energy-efficient near room-temperature thermal control of spacecrafts, Sol. Energy Mater. Sol. Cells 117 (2013) 494–498, https://doi.org/10.1016/j.solmat.2013.07.023.

[4] S. Corpino, M. Caldera, F. Nichele, M. Masoero, N. Viola, Thermal design and analysis of a nanosatellite in low earth orbit, Acta Astronaut. 115 (2015) 247–261, https://doi.org/10.1016/j.actaastro.2015.05.012.

[5] K. Sun, C.A. Riedel, A. Urbani, M. Simeoni, S. Mengali, M. Zalkovskij, B. Bilenberg, C.H. de Groot, O.L. Muskens, VO_2 thermochromic metamaterial-based smart optical solar reflector, ACS Photonics 5 (2018) 2280–2286, https://doi.org/10.1021/acsphotonics.8b00119.

[6] K. Kokini, Y.R. Takeuchi, B.D. Choules, Surface thermal cracking of thermal barrier coatings owing to stress relaxation: zirconia vs. mullite, Surf. Coat. Technol. 82 (1996) 77–82, https://doi.org/10.1016/0257-8972(95)02647-9.

[7] P. Ramaswamy, S. Seetharamu, K.J. Rao, K.B.R. Varma, Thermal shock characteristics of plasma sprayed mullite coatings, J. Therm. Spray Technol. 7 (1998) 497–504, https://doi.org/10.1361/105996398770350710.

[8] V. Heydari, Z. Bahreini, M. Heidari, A. Sedrpoushan, Synthesis of Zn-SBA-15 as a new pigment for spacecraft white thermal control coatings, J. Coat. Technol. Res. 13 (2016) 727–733, https://doi.org/10.1007/s11998-015-9778-9.

[9] M.M. Mikhailov, V.Y. Ul'yanitskii, V.A. Vlasov, A.N. Sokolovskiy, A.A. Lovitskii, Thermostabilizing $BaTiO_3$ coatings synthesized by detonation spraying method, Surf. Coat. Technol. 319 (2017) 70–75, https://doi.org/10.1016/j.surfcoat.2017.03.069.

[10] M. Takesue, H. Hayashi, R.L. Smith, Thermal and chemical methods for producing zinc silicate (willemite): a review, Prog. Cryst. Growth Charact. Mater. 55 (2009) 98–124, https://doi.org/10.1016/j.pcrysgrow.2009.09.001.

[11] R. Ye, G. Jia, D. Deng, Y. Hua, Z. Cui, S. Zhao, L. Huang, H. Wang, C. Li, S. Xu, Controllable synthesis and tunable colors of α- and β-Zn_2SiO_4:Mn^{2+} nanocrystals for UV and blue chip excited white LEDs, J. Phys. Chem. C 115 (2011) 10851–10858, https://doi.org/10.1021/jp2023633.

[12] P. Avouris, T.N. Morgan, A tunneling model for the decay of luminescence in inorganic phosphors: the case of Zn_2SiO_4:Mn, J. Chem. Phys. 74 (1981) 4347–4355, https://doi.org/10.1063/1.441677.

[13] J. Zhou, J. Liu, X. Wang, J. Song, R. Tummala, N.S. Xu, Z.L. Wang, Vertically aligned Zn_2SiO_4 nanotube/ZnO nanowire heterojunction arrays, Small 3 (2007) 622–626, https://doi.org/10.1002/smll.200600495.

[14] L. Wang, X. Liu, Z. Hou, C. Li, P. Yang, Z. Cheng, H. Lian, J. Lin, Electrospinning synthesis and luminescence properties of one-dimensional Zn_2SiO_4:Mn^{2+} microfibers and microbelts, J. Phys. Chem. C 112 (2008) 18882–18888, https://doi.org/10.1021/jp806392a.

[15] F. Huang, D. Chen, Synthesis of Mn^{2+}:Zn_2SiO_4-Eu^{3+}:Gd_2O_3 nanocomposites for highly sensitive optical thermometry through the synergistic luminescence from lanthanide-transition metal ions, J. Mater. Chem. C 5 (2017) 5176–5182, https://doi.org/10.1039/c7tc01500c.

[16] K. Omri, O.M. Lemine, L. El Mir, Mn doped zinc silicate nanophosphor with bi-functionality of green-yellow emission and magnetic properties, Ceram. Int. 43 (2017) 6585–6591, https://doi.org/10.1016/j.ceramint.2017.02.091.

[17] C.E. Rivera-Enríquez, A. Fernández-Osorio, J. Chávez-Fernández, Luminescence properties of α- and β-Zn_2SiO_4:Mn nanoparticles prepared by a co-precipitation method, J. Alloy. Comp. 688 (2016) 775–782, https://doi.org/10.1016/j.jallcom.2016.07.266.

[18] S. Zhang, L. Ren, S. Peng, Zn_2SiO_4 urchin-like microspheres: controlled synthesis and application in lithium-ion batteries, CrystEngComm 16 (2014) 6195–6202, https://doi.org/10.1039/c4ce00479e.

[19] S. Zhang, M. Lu, Y. Li, F. Sun, J. Yang, S. Wang, Synthesis and electrochemical properties of Zn_2SiO_4 nano/mesorods, Mater. Lett. 100 (2013) 89–92, https://doi.org/10.1016/j.matlet.2013.03.021.

[20] S. Zhang, L. Hou, M. Hou, H. Liang, Hydrothermal synthesis of spindle-like Zn_2SiO_4 nanoparticles and its application in lithium-ion battery, Mater. Lett. 156 (2015) 82–85, https://doi.org/10.1016/j.matlet.2015.05.004.

[21] A. Forés, M. Llusar, J.A. Badenes, J. Calbo, M.A. Tena, G. Monrós, Cobalt minimisation in willemite ($Co_xZn_{2-x}SiO_4$) ceramic pigments, Green Chem. 2 (2000) 93–100, https://doi.org/10.1039/b000748J.

[22] H. Cui, M. Zayat, D. Levy, Nanoparticle synthesis of willemite doped with cobalt ions ($Co_{0.05}Zn_{1.95}SiO_4$) by an epoxide-assisted sol-gel method, Chem. Mater. 17 (2005) 5562–5566, https://doi.org/10.1021/cm051289s.

[23] E. Ozel, H. Yurdakul, S. Turan, M. Ardit, G. Cruciani, M. Dondi, Co-doped willemite ceramic pigments: technological behaviour, crystal structure and optical properties, J. Eur. Ceram. Soc. 30 (2010) 3319–3329, https://doi.org/10.1016/j.jeurceramsoc.2010.08.013.

[24] A.E. Lavat, G.X. Gayo, In situ formation of coloured M(II)-doped Zn_2SiO_4-willemite in ceramic glazes (M = Mn, Co, Ni, Cu), Ceram. Int. 40 (2014) 11947–11955, https://doi.org/10.1016/j.ceramint.2014.04.031.

[25] X. Wang, H. Huang, B. Liu, B. Liang, C. Zhang, Q. Ji, D. Chen, G. Shen, Shape evolution and applications in water purification: the case of CVD-grown Zn_2SiO_4 straw-bundles, J. Mater. Chem. 22 (2012) 5330–5335, https://doi.org/10.1039/c1jm14551g.

[26] Y. Yang, Y. Zhuang, Y. He, B. Bai, X. Wang, Fine tuning of the dimensionality of zinc silicate nanostructures and their application as highly efficient absorbents for toxic metal ions, Nano Res. 3 (2010) 581–593, https://doi.org/10.1007/s12274-010-0019-3.

[27] M. Wu, L. Shi, T.T. Lim, A. Veksha, F. Yu, H. Fan, J. Mi, Ordered mesoporous Zn-based supported sorbent synthesized by a new method for high-efficiency desulfurization of hot coal gas, Chem. Eng. J. 353 (2018) 273–287, https://doi.org/10.1016/j.cej.2018.07.134.

[28] C.C. Diao, C.F. Yang, Synthesis of high efficiency Zn_2SiO_4:Mn^{2+} green phosphors using nano-particles, Ceram. Int. 36 (2010) 1653–1657, https://doi.org/10.1016/j.ceramint.2010.02.034.

[29] P.V. Ramakrishna, D.B.R.K. Murthy, D.L. Sastry, Synthesis, structural and luminescence properties of Ti co-doped ZnO/Zn_2SiO_4:Mn^{2+} composite phosphor, Ceram. Int. 40 (2014) 4889–4895, https://doi.org/10.1016/j.ceramint.2013.10.065.

[30] D.K. Bharti, M.K. Gupta, A.K. Srivastava, Giant dielectric constant and band gap reduction in hydrothermal grown highly crystalline zinc silicate nanorods, Mater. Lett. 232 (2018) 66–69, https://doi.org/10.1016/j.matlet.2018.08.085.

[31] K. Xiong, J. Liu, J. Li, J. Ye, Microwave-assisted hydrothermal synthesis of sub-micrometer willemite phase zinc silicate and its zinc ion release behavior, J. Am. Ceram. Soc. 96 (2013) 657–664, https://doi.org/10.1111/jace.12027.

[32] M. Takesue, A. Suino, Y. Hakuta, H. Hayashi, R.L. Smith, Formation mechanism and luminescence appearance of Mn-doped zinc silicate particles synthesized in supercritical water, J. Solid State Chem. 181 (2008) 1307–1313, https://doi.org/10.1016/j.jssc.2008.02.036.

[33] S. Toyama, M. Takesue, T.M. Aida, M. Watanabe, R.L. Smith, Easy emission-color-control of Mn-doped zinc silicate phosphor by use of pH and supercritical water conditions, J. Supercrit. Fluids 98 (2015) 65–69, https://doi.org/10.1016/j.supflu.2015.01.007.

[34] C.C. Lin, P. Shen, Sol-gel synthesis of zinc orthosilicate, J. Non-Cryst. Solids 171 (1994) 281–289, https://doi.org/10.1016/0022-3093(94)90197-X.

[35] T.S. Ahmadi, M. Haase, H. Weller, Low-temperature synthesis of pure and Mn-doped willemite phosphor (Zn_2SiO_4:Mn) in aqueous medium, Mater. Res. Bull. 35 (2000) 1869–1879, https://doi.org/10.1016/S0025-5408(00)00391-3.

[36] P. Švančárek, R. Klement, D. Galusek, Photoluminescence of $(ZnO)_{X-Z}(SiO_2)_Y$:$(MnO)_Z$ green phosphors prepared by direct thermal synthesis: the effect of ZnO/SiO_2 ratio and Mn^{2+} concentration on luminescence, Ceram. Int. 42 (2016) 16852–16860, https://doi.org/10.1016/j.ceramint.2016.07.176.

[37] S.R. Lukić, D.M. Petrović, M.D. Dramićanin, M. Mitrić, L. Dačanin, Optical and structural properties of Zn_2SiO_4:Mn^{2+} green phosphor nanoparticles obtained by a polymer-assisted sol-gel method, Scr. Mater. 58 (2008) 655–658, https://doi.org/10.1016/j.scriptamat.2007.11.045.